

Structural and Hydrodynamic Model Testing of the Transverse Horizontal Axis Water Turbine

R.A. McAdam^{#1}, G.T. Housby^{#2}, M.L.G. Oldfield^{#3}

[#] *Department of Engineering Science, University of Oxford
Parks Road, Oxford OX1 3PJ, UK*

¹ross.mcadam@eng.ox.ac.uk

²guy.housby@eng.ox.ac.uk

³martin.oldfield@eng.ox.ac.uk

Abstract— Model tests on two designs of 0.5m diameter transverse flow turbine are described. Measurements were made relevant to both the hydrodynamic and structural performance of the turbines, and a variety of conditions were explored (including flow depth, upstream velocity, flow direction, blade pitch, turbine solidity). This paper concentrates particularly on the measurements of loads on the turbine blades.

Keywords— Tidal power, turbine, transverse flow, fluid loading, stresses

NOMENCLATURE

A	Turbine area
b	Test section width
$B = A/hb$	Blockage ratio
c	Blade chord
$C_L = w/\frac{1}{2}c\rho(\lambda u)^2$	Equivalent lift coefficient
$C_P = P/\frac{1}{2}\rho Au^3$	Power coefficient
$C_T = T/\frac{1}{2}\rho Au^2$	Thrust coefficient
$Fr = u/\sqrt{gh}$	Froude number
g	Gravitational acceleration
h	Flow depth
N	Number of blades
P	Power generated
R	Turbine radius
$S = Nc/2\pi R$	Turbine solidity
T	Thrust on the turbine
u	Velocity at the test section
w	Radial load per unit length
$\lambda = \omega R/u$	Tip Speed Ratio (TSR)
ρ	Fluid density
ω	Turbine angular velocity.

I. INTRODUCTION

While the axial-flow turbine has been widely adopted in the tidal stream industry [1], the scale of such devices is limited by the channel depth at a given tidal location [2]. The Transverse Horizontal Axis Water Turbine (THAWT) is a

variant of a Darrieus turbine and has been proposed as an alternative design of tidal energy convertor, which can be more easily scaled by stretching the device across a channel. The turbine is configured with the rotation axis horizontal and perpendicular to the flow. The key feature of the turbine is that the blades are angled and connected to form a structurally stiff truss (Fig. 1). During March-April 2008 a series of tests was carried out on a 0.5 m diameter model THAWT at Newcastle University [3], [4]. These tests were successful in demonstrating that parallel and truss configurations of the THAWT device were capable of exceeding the Lanchester-Betz limit of kinetic power coefficient, used in wind turbine theory, by using blockage effects. Further variations in the device configuration were explored and indicated that the performance of the device was significantly improved by applying a negative 2° fixed offset pitch to the blades. Negative pitch decreases the angle of attack on the upstream side of the turbine with the blade leading edge moved away from the turbine axis, compared to the trailing edge.

A second series of tests were carried out in December 2010 – January 2011, with the following purposes:

- To provide further verification of the hydrodynamic performance of the turbine,
- To provide detailed information on loads on turbine blades, to allow structural design of a full scale turbine,
- To provide more detailed characterisation of the flow around and downstream of the turbine,
- To provide information that would allow further optimisation of design.

As in the previous tests, two main turbine configurations were tested, a “Parallel bladed” device (Fig. 2), which is essentially a standard Darrieus Turbine and a “Truss” THAWT device consisting of three bays (Fig. 1). This latter turbine is more representative of a 5 or 6 bay full-size rotor than the single bay rotor tested in 2008.

Over 170 tests were completed, including calibration tests. In this paper we report some of the hydrodynamic results, but concentrate mainly on the measurements of loads in the blades, as this is the area of most novelty.



Fig. 1 The 3-bay truss THAWT turbine.



Fig. 2 The parallel bladed turbine.

II. TEST SET-UP AND PROCEDURES

The flume used for these tests is located at the School of Marine Science and Technology at Newcastle University. It is 1.8m wide and allows flows up to 1.0 m deep (1.0 m and 0.8 m were used in this testing programme). The maximum flow velocity used in these tests was approximately 0.6 m/s. The testing section of the flume is about 11.2 m long, and in these tests the turbine centreline was placed 5.3 m from the upstream end of the flume. A streamlined constriction, housing the bearings and power take-off belt drive, was present at the turbine location, narrowing the flume locally from 1.8m to 1.61m. The length of both designs of turbine rotor was 1.55 m, with a small gap at either side to prevent drag due to wall shear. A speed controlled servo motor/generator was used to slowly ramp the rotor speed up and down to sweep through the operating speed range.

Several types of instrumentation were used. A comprehensive description of each device is not possible here, but the principle measurements were as follows.

The depth of water in the flume was measured continuously at up to three locations with capacitive “wave probes” which were logged at approximately 60 Hz.

The velocity at one point in the flume was measured by a “Vectrino” probe (based on the acoustic Doppler principle), which provides measurement of all three components of velocity at approximately 60 Hz.

An Acoustic Doppler Current Profiler (ADCP) was used to measure a profile of streamwise velocity at one plan location. This gave a profile of velocity through the depth of the flume at 10 mm vertical intervals. The ADCP was usually deployed downstream of the turbine to measure conditions in the wake, but was also traversed across the flume to provide detailed information about the flow conditions across the full cross-section of the flume.

The angular position of the turbine was measured with a shaft-encoder.

A single transducer provided measurement of torque and angular velocity. This device was located on the input shaft to the motor/generator used for power take-off, and so the measurements of torque include any losses in the transmission system, which were later calibrated out.

Strain gauges (deployed in full bridge, temperature compensated configurations) were used to measure the bending moment at four points along one of the blades in the Parallel turbine. These four measurements of bending moment were fitted by a best-fit parabolic function of distance along the blade, and the bending moments at the ends and mid-point deduced. By differentiating the bending moment twice one can deduce the distributed radial load, which is fitted as constant along the length of blade. (An alternative procedure was also examined in which a cubic was fitted exactly to the four measurements, implying a linear variation of radial load: this procedure resulted in over-fitting of the data, and was excessively sensitive to small variations in any one reading.) The bending moment measurements were made at approximately 2 kHz, and so provide a detailed picture of the variation of the radial load with angular position.

On the Truss turbine, strain gauges were used to measure bending moment at three points, thus allowing a parabolic variation of bending moment to be determined. Again the implied distributed load can only be represented as constant along the length of the blade, which will be an approximation only, as in this case the two ends of the blade are at different points in the angular cycle. On this blade a fourth bridge was used to measure the blade tension. The instrumented blade could be deployed in either the central bay or one of the end bays of the turbine. The gauges can be seen in the middle bay in Fig. 1.

A strain gauged load cell was used to measure the thrust in the downstream direction exerted by the turbine on the supporting bearing. The total thrust is estimated as twice this value, assuming equal thrusts at the two ends of the turbine.

Each device was logged electronically. Because the logging rate for different devices was different, all logged data was time-stamped to allow different readings to be properly registered.

III. TEST PROGRAMME AND PROCEDURES

The test programme consisted of two groups of tests on (a) the Parallel bladed device and (b) the Truss device. The former were directed mainly towards providing a deeper scientific understanding of the turbine mechanics, whereas the

latter were to demonstrate the performance of the full multi-bay truss under a variety of conditions.

In the following we express the results as far as possible in dimensionless terms, using the Froude number Fr , tip speed ratio (TSR) λ , blockage ratio B , turbine solidity S , power coefficient C_P and thrust coefficient C_T , as expressed in equations 1 – 6.

$$Fr = u/\sqrt{gh} \quad (1)$$

$$\lambda = \omega R/u \quad (2)$$

$$B = A/hb \quad (3)$$

$$S = Nc/2\pi R \quad (4)$$

$$C_P = P/\frac{1}{2}\rho Au^3 \quad (5)$$

$$C_T = T/\frac{1}{2}\rho Au^2 \quad (6)$$

Each test involved gradually ramping up the angular velocity from zero, through the velocity at which peak power was achieved and continuing to a sufficiently high velocity that power was absorbed rather than generated. The TSR at which the net power falls to zero is termed the free-running TSR. The velocity was then slowly reduced back to zero. All instrumentation was logged continually. The result was a complete mapping of the power curve twice (once for increasing TSR and once for decreasing). The actual command velocity was not always achieved exactly, with the result that at some stages the velocity would undergo a relatively rapid transition from one value to another. In these cases the increasing and decreasing TSR sections of the power curve tend to differ, (see Fig. 7, discussed below).

A. Parallel tests

For the Parallel tests the following effects were examined:

- Effect of flow velocity (expressed in terms of Froude number). For all other conditions equal, several tests were conducted at different flow velocities. This study was carried out for different blockage ratios and for forward and reverse flow.
- Effect of blockage ratio. Tests were carried out at depths of 1.0 m and 0.8 m ($B = 0.43, 0.54$).
- Effect of “forward” and “reverse” rotation. Forward rotation is defined as the case where the bottom of the turbine is moving in the same direction as the flow.
- Effect of blade pitch angle. The “standard” blade pitch angle was -2° (determined from the previous testing series). Tests were carried out at a variety of pitches between 0° and -6° . These tests were carried out for a variety of conditions (different flow velocities and depths).
- Effect of number of blades. Tests were carried out for 3, 4, 5 and 6 blades. These tests can also be regarded as tests on the effects of the solidity S of the turbine.

B. Truss tests

For the Truss tests the number of blades is always 6 in any one bay, and the pitch angle was fixed at -2° , so only the first three of the above studies were carried out for the truss.

IV. NUMERICAL ANALYSES

The test results are compared with numerical predictions. The experience from the previous experiments was that a combination of Blade Element Theory with the “Modified Betz” theory [5] provided a prediction which was qualitatively correct but systematically over predicted the power output. This was attributed principally to the observation that the flow through the downstream side of the turbine is slowed significantly as the flow diverges through the device.

The previous tests [4] had, however, been quite well modelled retrospectively using a two dimensional numerical model in which a quasi-steady-state solution is developed. In the analysis the turbine is replaced by an annulus in which time-averaged body forces are applied to represent the appropriate hydrofoil lift and drag characteristics, representing the blades in a “smeared” manner (see Fig 3). Although this is a simplification, it does, as will be shown, capture the flow through the rotor in a manner which gives an understanding of the rotor performance. A brief description of the method used is given here. A grid converged finite-element Navier-Stokes approach was used to solve the flow domain, with non-slip and symmetry boundary conditions applied to the flume base and free surface respectively. Isotropic and SUPG [6] added viscosity have been used to stabilise oscillations in the solution, but are anticipated to be sufficiently low as to have little effect on the accuracy of the solution. A turbulence model has not been applied to the problem, which is anticipated to induce errors in the wake mixing and bed velocity profile development. However, these errors are expected to be negligible when compared to the accuracy of the actuator cylinder approach. This method was used to predict the results of the experiments. The numerical analysis was implemented in COMSOL (a commercial multiphysics simulation software package, see <http://www.comsol.com>).

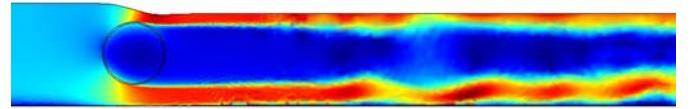


Fig.3 Velocity contour plot produced in COMSOL of the THAWT device with a blockage of $B = 0.625$, $Fr = 0.19$ and free surface deformation. High speed flow regions are shown in red and low speed regions in dark blue. The turbine is represented by the circle on the left.

The numerical analyses could be carried out in two modes: either an iterative analysis in which the position of the free surface is established, or a (much faster) analysis using an approximate “rigid lid” model with constant depth. The latter is appropriate, provided depth changes are not too large. The implied depth change can be deduced from the pressure change $\delta h \approx \delta p/\rho g$. The numerical model does not take into account blade sweep angle, so must be regarded as a model of the parallel turbine only.

The numerical analyses were carried out for a flume with parallel sides. Comparisons between experimental results and numerical analyses are made in terms of the local accelerated velocity through the flow constriction at the turbine.

The numerical analyses were carried out for blockage ratios of 0.5 and 0.625. For both cases analyses were carried out at a variety of velocities. For $B = 0.5$, further studies were carried out to examine the effects of the solidity and blade pitch angle. The results of the numerical analyses are summarised in Table 1, and the conclusions are as follows:

- 1) A typical power v . TSR plot is given in Fig. 4. Peak power was predicted at a TSR of typically 2.8 for the tests at $B = 0.5$ and 3.3 at $B = 0.625$. The TSR at peak power also decreases slightly with increasing flow velocity. Converged analyses could not be obtained for the unstable branch of the power curve (TSR below about 2.0).
- 2) Zero power was predicted at a TSR of about 4.2 for $B = 0.5$ and 5.2 for $B = 0.625$.
- 3) Peak power coefficient was found to increase slightly with Froude number, and was higher for the higher B value.
- 4) The thrust coefficients at peak power are remarkably independent of Froude Number, but do depend on B .
- 5) The dimensionless depth change at peak is a strong function of Froude number and also of B .
- 6) The power coefficient reduces slightly with increased solidity S .
- 7) The power coefficient is a mild function of the blade pitch, with the optimal power occurring at a pitch of around -2° to -3° .
- 8) The predicted radial blade loading shows a characteristic variation with angular position θ , illustrated in Fig. 5 for typical conditions at peak power. The radial load per unit length w is expressed in terms of an equivalent lift coefficient, as shown in eq. 7.

$$C_L = \frac{w}{\frac{1}{2}c\rho(\lambda u)^2} \quad (7)$$

The minimum (*i.e.* maximum towards the blade axis) load occurs at $\theta \approx 90^\circ$, at the upstream side of the turbine. The maximum outward load occurs typically at $\theta \approx 350^\circ$, just before the blade reaches the top of the cycle in forward rotation. The force vectors are also illustrated in Fig. 6, showing a vector representing the magnitude and direction of the force exerted on the blades at each point around the cycle. Especially at $\theta \approx 90^\circ$, the component of the force in the sense of the rotation, giving rise to positive power, can easily be seen.

TABLE I
SUMMARY OF RESULTS OF NUMERICAL ANALYSES

		← Peak conditions →							Free run.
B	Pitch	S	Fr	TSR	C_p	C_T	$\delta h/h$	TSR	
Effect of Froude Number	0.625	-2°	0.25	0.089	3.4	1.203	3.643	0.010	5.0
	0.625	-2°	0.25	0.100	3.4	1.257	3.670	0.013	5.2
	0.625	-2°	0.25	0.107	3.4	1.290	3.686	0.015	5.2
	0.625	-2°	0.25	0.125	3.2	1.386	3.601	0.020	5.2
	0.625	-2°	0.25	0.139	3.2	1.440	3.625	0.025	5.2
	0.625	-2°	0.25	0.143	3.2	1.440	3.620	0.027	5.2
	0.625	-2°	0.25	0.161	3.2	1.460	3.612	0.034	5.4
	0.625	-2°	0.25	0.178	3.2	1.476	3.601	0.044	5.4
	0.5	-2°	0.25	0.096	2.9	0.718	2.514	0.007	4.1
	0.5	-2°	0.25	0.109	2.9	0.718	2.440	0.009	
	0.5	-2°	0.25	0.128	2.7	0.811	2.458	0.015	4.3
	0.5	-2°	0.25	0.144	2.7	0.832	2.468	0.017	
	0.5	-2°	0.25	0.160	2.7	0.863	2.465	0.021	4.3
	0.5	-2°	0.25	0.176	2.7	0.873	2.461	0.024	
0.5	-2°	0.25	0.179	2.7	0.870	2.460	0.028		
0.5	-2°	0.25	0.192	2.7	0.883	2.456	0.031		
Effect of Solidity	0.5	-2°	0.125	0.128	3.4	1.000	2.139	0.011	6.0
	0.5	-2°	0.167	0.128	3.1	0.960	2.306	0.012	
	0.5	-2°	0.208	0.128	2.9	0.887	2.408	0.012	
	0.5	-2°	0.25	0.128	2.7	0.811	2.458	0.015	4.3
	0.5	-2°	0.125	0.144	3.4	0.989	2.133	0.014	6.0
	0.5	-2°	0.167	0.144	3.1	0.951	2.300	0.015	
	0.5	-2°	0.208	0.144	2.9	0.894	2.411	0.016	
	0.5	-2°	0.25	0.144	2.7	0.832	2.468	0.017	
Effect of Pitch	0.5	-1°	0.25	0.160	2.5	0.856	2.423	0.021	
	0.5	-2°	0.25	0.160	2.7	0.863	2.465	0.021	4.3
	0.5	-3°	0.25	0.160	2.5	0.858	2.369	0.021	4.1
	0.5	-4°	0.25	0.160	2.5	0.836	2.346	0.020	3.9
	0.5	-5°	0.25	0.160	2.5	0.776	2.317	0.020	3.9
	0.5	-6°	0.25	0.160	2.5	0.635	2.315	0.019	3.7
	0.625	-2°	0.25	0.089	3.4	1.203	3.643	0.010	5.0
	0.625	-2°	0.25	0.100	3.4	1.257	3.670	0.013	5.2

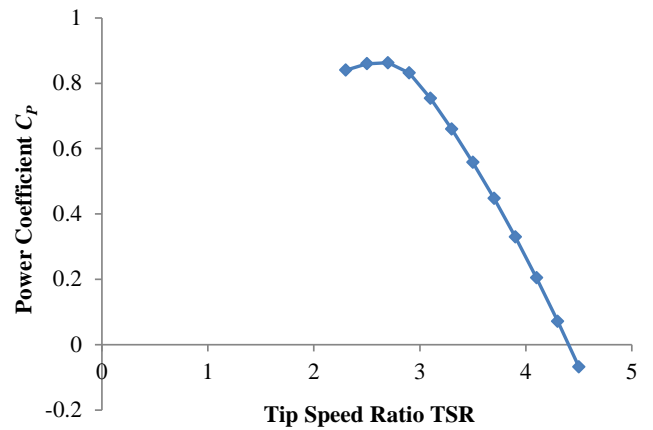


Fig.4 Power coefficient v . Tip Speed Ratio from numerical analysis, $B = 0.5$, $Fr = 0.178$

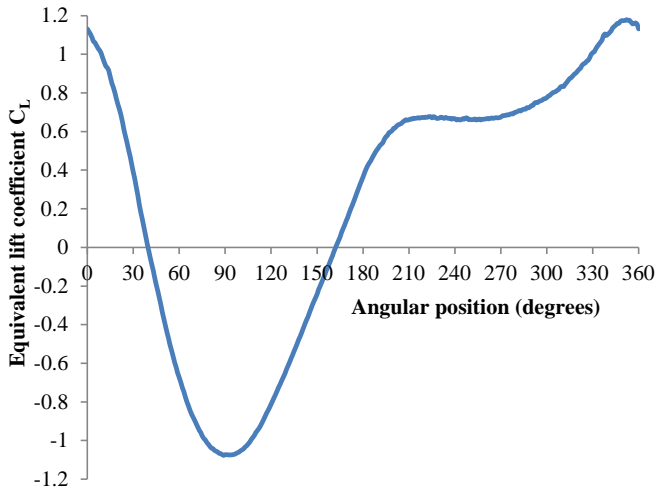


Fig. 5 Variation of radial force (expressed as equivalent lift coefficient) with angular position, peak power, $B = 0.5$, $Fr = 0.178$

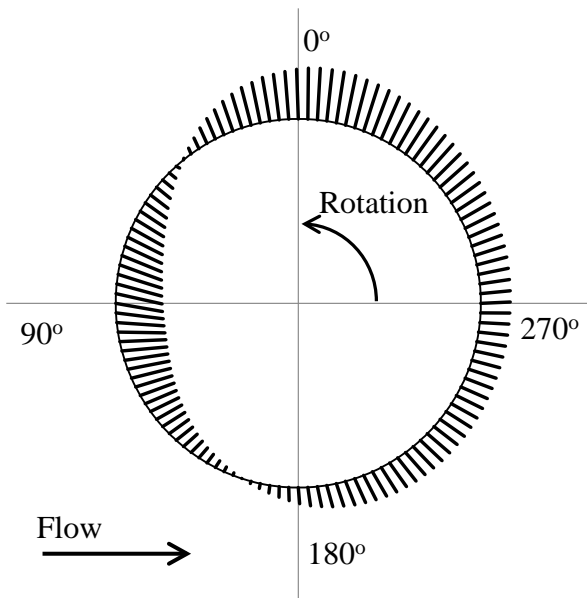


Fig. 6 Computed force vectors around the turbine

It is important to realise the limitations of the simplified numerical analysis, which is intended as approximate only. In particular it replaces a time varying problem with a time-averaged equivalent, and the effect of wake mixing is anticipated to have little effect on the accuracy of the solution.

V. EXPERIMENTAL RESULTS

Fig. 7 shows a typical measured power coefficient ν . TSR plot from a test on the Parallel bladed turbine. The points are plotted at 1second intervals. For most of the TSR range, the slow change in TST ensured quasi-steady operation and the increasing and decreasing speed plots overlaid each other. However, a rapid transition on both the upward (from approx. $TSR = 1.5$) and downward (from approx. $TSR = 2.5$) branches of the curve can be seen, with progress of the measured path illustrated by the blue arrows. In this region the control algorithm was unable to track the unstable section of the

power curve, and quasi-steady flow was not maintained. The “true” curve is likely to be close to the red dashed line.

The measured peak power coefficients are compared with the numerical analyses (lines of best fit shown as continuous curves) in Fig. 8. Comparisons are made in terms of the flow conditions through the narrowed section of the flume at the turbine. The experimental values have been corrected by calibrations for small losses in the transmission system, and for drag on the turbine end-plates. At the lower blockage ratio there is very close agreement between experiment and analysis, with slightly lower measured power coefficient (compared to the analysis) at lower Froude numbers, and slightly higher values at higher Fr . There is no discernable difference between forward and reverse rotation. At the higher blockage ratio the numerical analysis predicts higher powers than those measured, and forward rotation gives a distinctly better performance than reverse, probably due to the accelerated flow passing over the top of the turbine. Note, however, that all the measured power coefficients are higher than the Betz limit, as would be expected from the analysis of Houlsey *et al.* [5].

The measured thrust coefficients (Fig. 9) also compare closely with the analysis, with the thrusts typically being somewhat lower than the predictions. The depth changes that occur across the turbine were measured. Assuming that these are primarily due to the turbine thrust, and assuming full mixing of the wake, the net depth change can be calculated from momentum theory, as shown in eq. 8.

$$-\frac{\delta h}{h} \approx \frac{T}{\rho g h^2 b (1 - u^2 / gh)} \quad (8)$$

Figure 10 shows the comparison between measured and calculated depth changes. The measured values are typically equal to, or slightly in excess of, the values calculated from the thrust, with the difference likely to be attributable to incomplete mixing (and hence incomplete depth recovery) before the downstream measurement point. A longer flume may have allowed fuller depth recovery. The same is true of the numerical analyses, in which a more distant downstream boundary may have been required.

The measured trends of variation of peak power with pitch angle and with solidity (not presented here) followed the predictions of the numerical analyses very closely.

The hydrodynamic measurements using the Truss turbine followed a very closely similar pattern to those reported here for the Parallel bladed device, except that the observed power was slightly lower. This is principally because of (a) the sweep angle of the blades which slightly reduces their efficiency and (b) for the Truss device, the measured power was inclusive of all parasitic drag on the structural elements between the turbine bays and at the ends of the turbine.

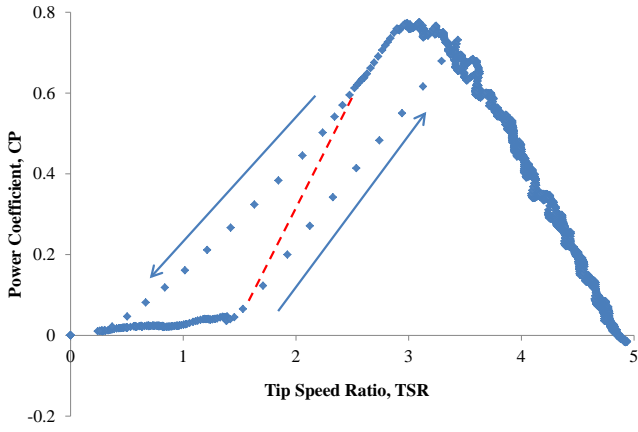


Fig. 7 Power coefficient v. Tip Speed Ratio, $B = 0.48$, $Fr = 0.143$

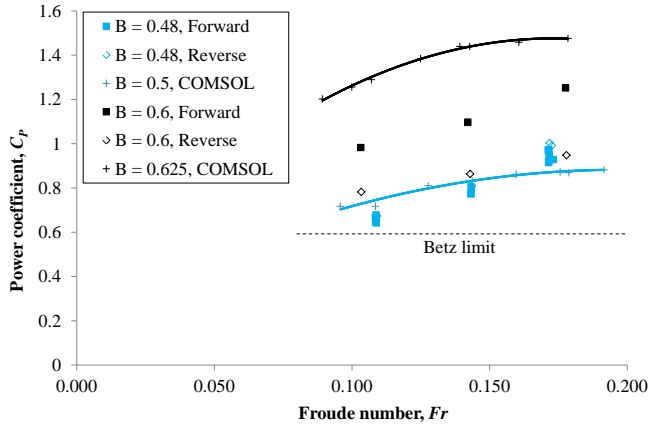


Fig. 8 Results of Parallel tests: power coefficient v. Froude number (all tests with $S = 0.25$, Pitch = -2°), lines of best fit shown with continuous curves

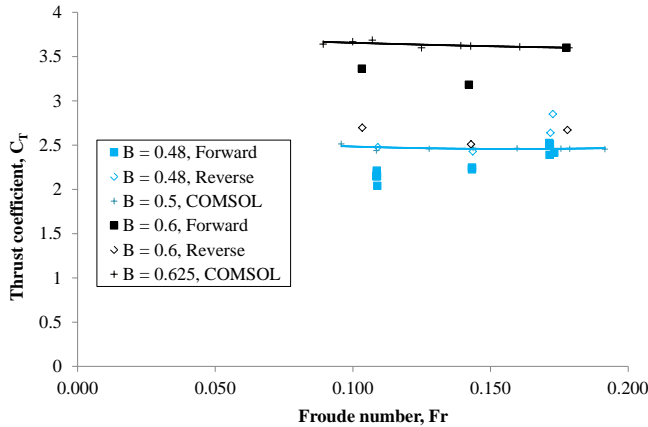


Fig. 9 Results of Parallel tests: thrust coefficient v. Froude number (all tests with $S = 0.25$, Pitch = -2°), lines of best fit shown with continuous curves

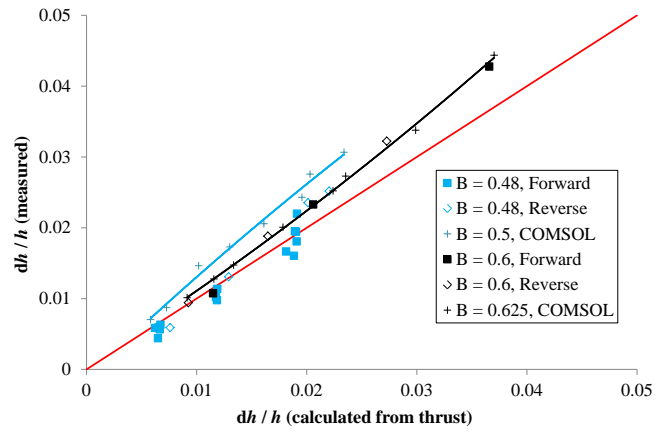


Fig. 10 Results of Parallel tests: measured depth change v. depth change expected from thrust measurements (all tests with $S = 0.25$, Pitch = -2°), lines of best fit shown with continuous curves

VI. LOAD MEASUREMENTS

One of the primary purposes of the tests was to measure the loads on the turbine blades as they vary around the cycle, in order to validate the approximate predictions from the numerical analyses as shown in Fig. 5.

Figure 11 shows the measured bending moment at the ends and centre of the blade in a test of the Parallel device, in which the bending moments at four measurement points have been fitted by a best-fit parabola and the values at ends and centre deduced. It can be seen that at any point in the cycle the bending moments at the ends are approximately equal (End 2 consistently slightly higher), of opposite sign to the central BM and approximately twice the magnitude. This is consistent with the blade acting as a built-in beam, in which the central and end bending moments would be $wL^2/24$ and $wL^2/12$. The slight asymmetry in the end moments may be due to variations in end fixity, or due to a slight asymmetry of flow in the flume.

By differentiating the bending moment twice the distributed load w can be deduced, with the parabolic variation of BM along the blade implying a constant value of w . This value is plotted in Fig. 12. It is seen that the pattern of load variation is remarkably similar to that shown in Fig. 5, including the location of both the maximum and minimum values, as well as the characteristic shape of the plot. This result lends confidence to both the numerical analyses and the test results.

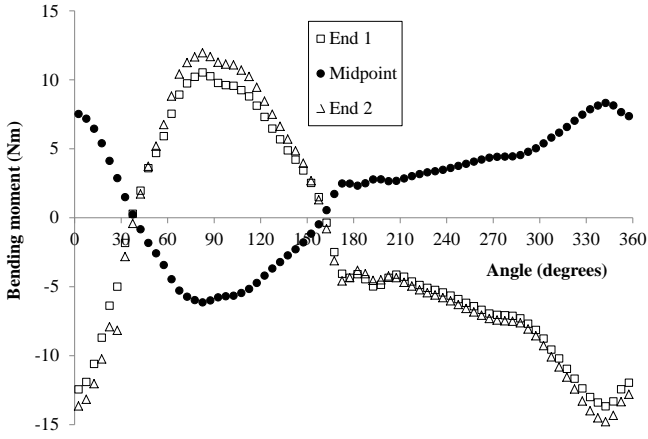


Fig. 11 Measurements of bending moment at peak power for test at $B = 0.48$, $Fr = 0.143$, $S = 0.25$, Pitch = -2°

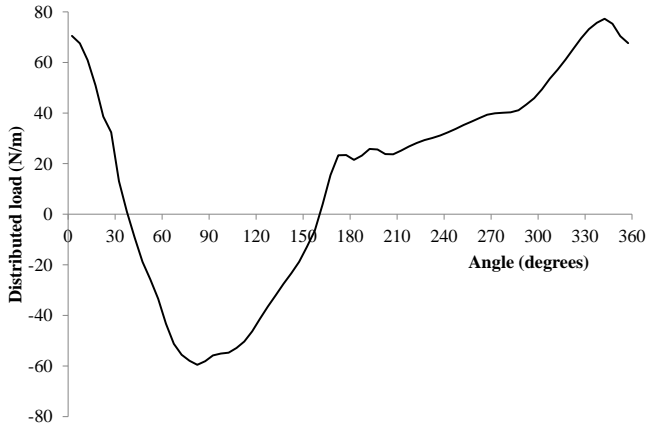


Fig. 12 Distributed load at peak power for test at $B = 0.48$, $Fr = 0.143$, $S = 0.25$, Pitch = -2°

From each test the maximum and minimum radial loads in the cycle at peak power are picked out, and converted to equivalent dimensionless lift coefficients, as described in eq. 7 (Note that this does not represent a true lift coefficient, as the value λu only represents an approximation to local flow velocity past the blade, and furthermore the force used is the radial force, not the force perpendicular to the relative velocity vector). These values are plotted in Fig. 13 as a function of Froude number. Whilst the numerical analyses give peak lift coefficients in the region of 1.0, the experiments indicate maximum values about 80% larger and minimum values about 60% larger. The explanation lies partly in the fact that the experimental data show higher peaks relative to the mean values, and partly in the fact that in the experiments peak power was observed at a somewhat lower TSR than in the analyses, so that the normalising factor used in deriving C_L is smaller.

Broadly similar conclusions can be drawn from the distributed load measurements made on the Truss tests. However, for the latter it was also possible to measure the tension in the blade. For this purpose the instrumented blade could be located either in one of the end bays, or in the middle bay of the truss. Figure 14 shows the variation of tension with angular position of the blade for a test in which the blade was

placed in an end bay. The variation of tension shows, as expected, a similar pattern to the variation of the loading, but with a somewhat smoother curve as the tensions are the result of the integration of the loading over the whole truss. Figure 15 shows the maximum and minimum tensions measured in the middle bay, at peak power, presented using the same normalisation factor as for the turbine thrust, *i.e.* $T/\frac{1}{2}\rho Au^2$.

It is seen that the normalised tensions are of the order of ± 1 , and that they increase only slightly with Froude number. The absolute value of the tension clearly depends on the blade position and turbine geometry, especially the length to diameter ratio.

The maximum tensions can also be compared directly with the thrust on the turbine, since the tension in the mid-bay arises principally from the overall lateral loading on the turbine. When this comparison is made it is found that the maximum and minimum tensions in the central bay of this turbine were typically about 40% of the thrust value.

VII. CONCLUSIONS

A comprehensive series of experiments have been carried out on a horizontal axis, transverse flow turbine in a flume. Both a parallel-bladed and a three bay truss variant of the turbine were tested. Hydrodynamic and structural performance of the turbines were measured for a variety of conditions, including varying flow velocity, blockage ratio, turbine solidity and fixed pitch angle. Only a brief summary of the main test results is presented here. The power curves obtained were similar to those obtained in earlier tests [3] on a single bay THAWT turbine and are more representative of a full size rotor. The present load tests are new and will be used to predict stresses in a full size turbine. The results are shown to be consistent with a simplified numerical analysis, and differences have been highlighted in the paper. Much further analysis of the tests remains to be completed.

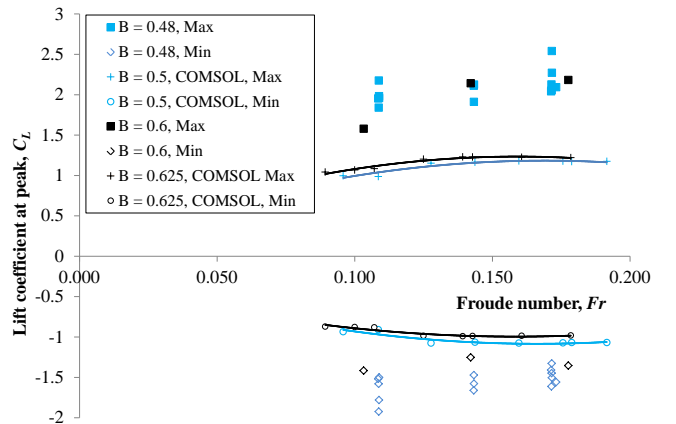


Fig. 13 Equivalent lift coefficient against Froude number for parallel blade tests

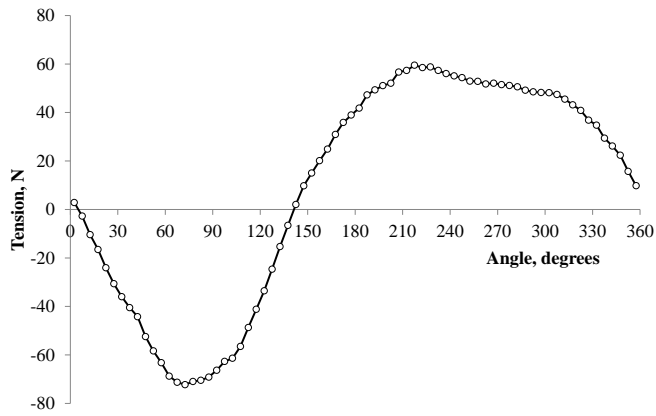


Fig. 14 Variation of tension in end bay with angle, peak power for Truss test at Froude number 0.144, blockage ratio 0.48

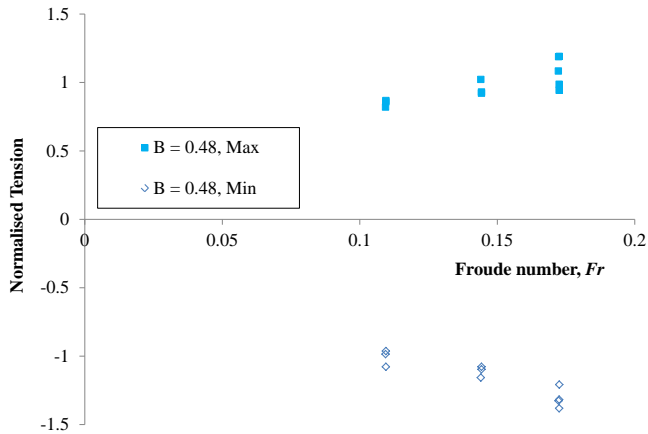


Fig. 15 Normalised tension, measured in middle bay

ACKNOWLEDGMENTS

This research was supported by the Technology Strategy Board under grant 001-12247 “Validating the Generic Application of an Innovative Second Generation Horizontal Axis Cross Flow Tidal Turbine”. The authors thank Kepler Energy Limited for permission to publish this paper. The authors are grateful for the assistance provided by the staff of the School of Marine Science and Technology at Newcastle University. The ADCP was supplied free of charge by Nortek under their graduate prize scheme.

REFERENCES

- [1] O'Rourke, F., Boyle, F. & Reynolds, A.: “Tidal energy update 2009”, *Applied Energy*, 2009, 87, (2), pp. 398-409.
- [2] Bryden, I. G., Naik, S., Fraenkel, P. & Bullen, C. R.: “Matching tidal current plants to local flow conditions”, *Energy*, 1998, 23, (9), pp. 699-709.
- [3] R.A. McAdam, G.T. Houlby, M.L.G. Oldfield. and M.D. McCulloch, "Experimental Testing of the Transverse Horizontal Axis Water Turbine", in *Proc. 8th European Wave and Tidal Energy Conference*, 2009, pp 360-365
- [4] R.A. McAdam, G.T. Houlby, M.L.G. Oldfield. and M.D. McCulloch, "Experimental Testing of the Transverse Horizontal Axis Water Turbine", *Proc. Institution of Engineering and Technology, Renewable Power Generation*, vol. 4, pp 510-518, 2010.
- [5] G.T. Houlby, S. Draper and M.L.G. Oldfield, "Application of Linear Momentum Actuator Disc Theory to Open Channel Flow", OUEL Report No. 2297/08, Department of Engineering Science, University of Oxford, 2008
- [6] Codina, R.: “Comparison of some finite element methods for solving the diffusion-convection-reaction equation”, *Computer Methods in Applied Mechanics and Engineering*, 1998, 156, (1-4), pp. 185-210.